JOURNAL OF MATERIALS SCIENCE 23 (1988) 2142–2152

# Characterization and study of $Na_2O$–$B_2O_3$–$SiO_2$ glasses prepared by the sol–gel method

M. A. VILLEGAS, J. M. FERNANDEZ NAVARRO
*Instituto de Cerámica y Vidrio, CSIC, Arganda del Rey, Madrid, Spain*

The sol–gel procedure has been used to prepare vitreous materials whose compositions are situated in the liquid–liquid immiscibility area of the $Na_2O$–$B_2O_3$–$SiO_2$ phase equilibrium diagram. Gels were prepared from different precursors and under different experimental conditions. After determining optimum conditions for gelling and heat-treatment, the gels were characterized with the aid of thermal analysis, X-ray diffraction, density and specific surface area measurements, as well as infrared and near-infrared spectroscopy. The textures of the samples and their microstructures were studied by means of scanning electron microscopy and transmission electron microscopy, respectively. The phase separation in the gels was compared to the same phenomenon in one of the glasses of identical composition, but prepared by conventional melting.

## 1. Introduction

The sol–gel method, which allows the preparation of glassy materials at low temperatures, has enjoyed increasing interest and further development in the last few years. The process owes its popularity mainly to the fact that it is a new and highly versatile method with many advantages, particularly for certain glass compositions which are difficult to prepare by conventional melting.

To date a considerable amount of research has been devoted to the polymerization of commercial colloidal silica or metalorganic silica compounds, such as tetraethylorthosilicate (TEOS) [1–8] and tetramethylorthosilicate (TMOS) [9–13], both oriented towards the study and preparation of pure silica glass. Other gels have also been prepared, mainly multicomponents [14–19]. A major part of these studies focused not only on the preparation of monolithic glasses, but also on fibres and thin coatings [20–24].

In only a few years several compositions of the system $Na_2O$–$B_2O_3$–$SiO_2$ [15, 18, 20, 25–29] have been obtained via sol–gel, as well as materials of other systems which contain, among others, silicon, boron and sodium oxides [14, 16, 30]. Some compositions are situated in the liquid–liquid immiscibility area of the phase equilibrium diagram. However, papers about studies of phase separation in these glasses are not very common. This phenomenon has been studied in glasses prepared from gels in other than $Na_2O$–$B_2O_3$–$SiO_2$ systems [31, 32].

This paper focuses on the preparation and study of vitreous borosilicate materials obtained by the sol–gel process. The $Na_2O$–$B_2O_2$–$SiO_2$ system was chosen for the interesting technical applications of several of its compositions (Pyrex and Vycor glasses) with regard to their well-known thermic and chemical properties. The compositions selected for this study are situated in the liquid–liquid immiscibility area of the phase equilibrium diagram (Fig. 1) for the purpose of studying the phase separation phenomenon by means of transmission electron microscopy (TEM). Furthermore the thermal evolution of the gels was studied by differential thermal analysis (DTA), X-ray diffraction, density and specific surface area measurements, as well as infrared (IR) and near-infrared (NIR) spectroscopy.

## 2. Experimental procedure

### 2.1. Sample preparation

For the purpose of this research, i.e. the study of potential phase separation in materials prepared by the sol–gel process in the $Na_2O$–$B_2O_3$–$SiO_2$ system, four compositions were chosen situated in the liquid–liquid immiscibility area of the phase equilibrium diagram (Table I).

TEOS was used as an $SiO_2$ source for all samples. The boron and sodium oxides sources were varied, yielding the combinations compiled in Table II.

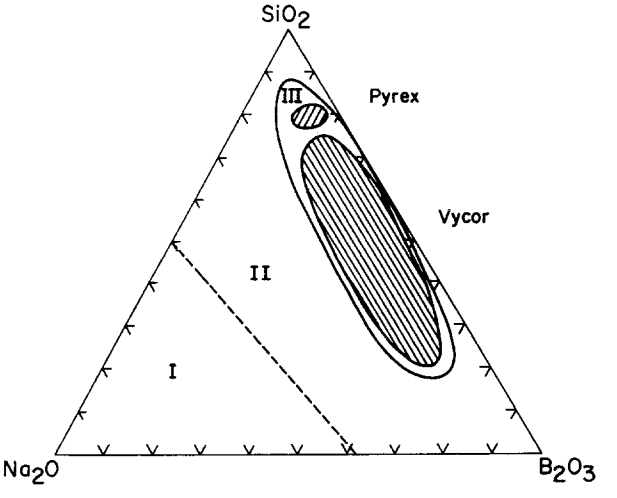


*Figure 1* Ternary diagram of the system $Na_2O$–$B_2O_3$–$SiO_2$. (I) crystallization area; (II) transparent glass area; (III) liquid–liquid phase separation area, favoured through heat-treatment.



0022–2461/88 $03.00 + .12 

TABLE I Compositions studied

| Composition No. | Composition (mol %) | | |
|---|---|---|---|
| | $Na_2O$ | $B_2O_3$ | $SiO_2$ |
| 4.1 | 5.78 | 15.60 | 78.62 |
| 4.2 | 5.59 | 12.36 | 82.05 |
| 4.3 | 5.45 | 9.29 | 85.26 |
| 4.4 | 5.30 | 6.38 | 88.32 |

TABLE II $B_2O_3$ and $Na_2O$ sources used in sample preparation

| Combination type | Precursors* |
|---|---|
| A | $NaNO_3$, $H_3BO_3$ |
| B | NaOEt, $H_3BO_3$ |
| C | NaOEt, $B(OMe)_3$ |
| D | $NaNO_3$, $B(OMe)_3$ |

*Et = $C_2H_5$, Me = $CH_3$.

The method used for the sol preparation was roughly the following:

(a) Silicon alkoxide hydrolysis with an amount of water approximately equivalent to the stoichiometric amount necessary for the hydrolysis of the alkoxide (molar ratio TEOS : $H_2O$ equal to 1:5). An acid catalyst (HCl) as well as ethanol equimolar to TEOS are added to the TEOS and water mixture.

(b) Addition of the $B_2O_3$ source.

(c) Addition of the $Na_2O$ source in aqueous solution.

In the tests performed, apart from varying the precursors different molar ratios were tested: TEOS : $H_2O$ started from a ratio of 1 : 10 upwards, TEOS : EtOH varied between 1 : 0.3 and 1 : 10, and the final pH of the sol ranged from 1 to 8.

The conditions chosen as a function of optimal properties achieved in the samples are listed below:

(i) precursors: $B(OMe)_3$ and $NaNO_3$ (Type D combination, Table II);
(ii) molar ratio TEOS : $H_2O$ = 1 : 10;
(iii) molar ratio TEOS : EtOH = 1 : 1;
(iv) final pH of the sol approximately 2.

For NIR spectra recordings (4000 to 10 000 $cm^{-1}$) thin planoparallel slabs were prepared in glass petri dishes, the thickness varying between 0.5 and 1 mm.

In addition to gels, conventional glass was prepared according to Composition 4.1. (Table I), from washed quartz sand, molten $B_2O_3$ and $Na_2CO_3$ through melting in an induction furnace and using a platinum crucible.

## 2.2. Gelation and heat-treatment

Once the sols had been prepared, they were heated mildly (40° to 60° C) or they were left to gel at room temperature, gelation taking place more slowly at lower temperatures.

The gels were allowed to dry for several days at low temperature and subsequently heat-treated according to pre-established heating and stabilization programmes (Fig. 2). Accelerated heat-treatment in the early stages of gel evolution proved inadequate for removal of organic groups as well as for the monolithic shape of the samples. It is recommended to dry the gels very slowly in order to avoid cracks and to prevent black particles from appearing as a result of carbonized organic groups during later treatments at higher temperatures. Drying the samples at low temperatures involves, however, the frequent risk of $NaNO_3$ surface crystallization, when segregated from the gel bulk. Drying times and heating rates should therefore not be so slow to favour the crystallization process.

The heat-treatments applied can be grouped as follows:

(a) drying heat-treatment prior to gel densification;
(b) heat-treatment of gels at higher temperatures;
(c) simultaneous heat-treatment of gels and glass (Composition 4.1) in order to induce phase separation.

Heat pre-treatment of the gels is but a slow drying process which eliminates the adsorbed water and the alcohols. The samples were submitted to several treatments at different temperatures up to 200° C. In the light of the end-features achieved in the samples, particularly their monolithicity, the following programme was chosen:

(i) heating rate 0.1° C $min^{-1}$ up to 120° C;
(ii) stabilization 13 h at 120° C;
(iii) heating rate 0.5° C $min^{-1}$ up to 200° C;
(iv) stabilization 13 h at 200° C.

For heat-treatment of the gels at higher temperatures many programmes were tested, varying the heating rates and stabilization times at different temperatures. In view of the results observed in the samples the following schedule was chosen:

(i) heating rate 1.25° C $min^{-1}$ up to 200° C;
(ii) stabilization 2 h at 200° C;
(iii) heating rate 1.25° C $min^{-1}$ up to 375, 550, 600 and 850° C;
(iv) stabilization 12 h at respective end-temperature.

The heat-treatments to induce phase separation in the gel and in the glass (Composition 4.1) consisted in heating at 600° C for 12 h and 700° C for 4 h; after this the samples were abruptly cooled to room

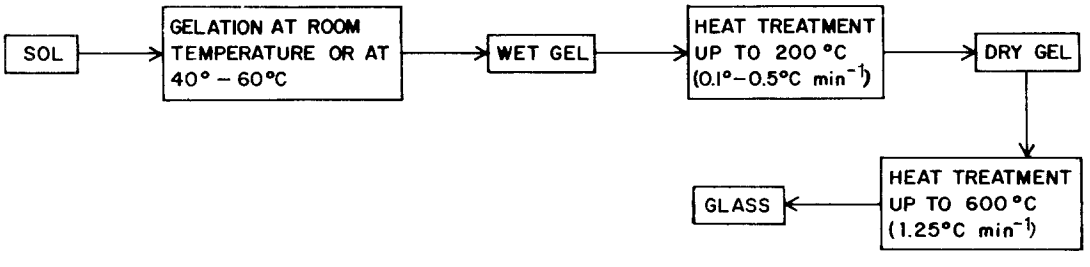


*Figure 2* Schematic representation of the sol–gel–glass evolution.

temperature and placed in a desiccator. In order to determine the temperature at which phase separation sets in for conventional glass, two heat-treatments at 500° C were performed for 2 h and 6.5 h, respectively, whereafter the sample was again abruptly cooled.

### 2.3. Gel characterization

The DTA and thermogravimetric analysis (TGA) diagrams were obtained on a Mettler instrument with a heating rate of 10° C $min^{-1}$ in a platinum crucible and with $Al_2O_3$ as reference substance.

The density of the samples was measured by Archimedes' method using toluene as immersion liquid. Each measurement was repeated four times for each treatment temperature.

Determination of the specific surface area of the gels was performed by means of the BET method on a Micromeritics apparatus, Model AccurSorb 2100 E.

The IR spectra were obtained from powder samples diluted in anhydrous KBr pellets on a Nicolet DX spectrophotometer. The respective NIR spectra were recorded on a Perkin–Elmer spectrophotometer, Model Lambda 9, using samples in the form of thin sheets.

The texture of the gels treated at 200° C was studied by scanning electron microscopy (SEM) on recently fractured surfaces. The samples treated at 500° C or higher temperatures were observed by transmission electron microscopy (TEM). The TEM samples were likewise prepared from a recent fracture which was HF-attacked for 30 sec.

## 3. Results and discussion

### 3.1. DTA–TGA diagrams and X-ray diffraction

The DTA–TGA diagrams for the samples (Fig. 3) show large endothermic peaks between 150 and 172° C, accompanied by significant weight losses in the respective TG curves. These endothermic effects are attributed to the loss of physically adsorbed water and alcohol. Approximately between 250 and 450° C, the TG curves drop due to the loss of water hydrogen-bonded to ≡Si–OH and =B–OH groups, as is confirmed by NIR spectroscopy (Section 3.3). In the temperature range between 531 and 550° C another endothermic effect is produced in the samples, again accompanied by a weight loss, however less marked than in the first event. This temperature range marks the onset of $OH^-$ release from the ≡Si–OH and =B–OH groups, which causes the network to close down, and the material begins to sinter, as is

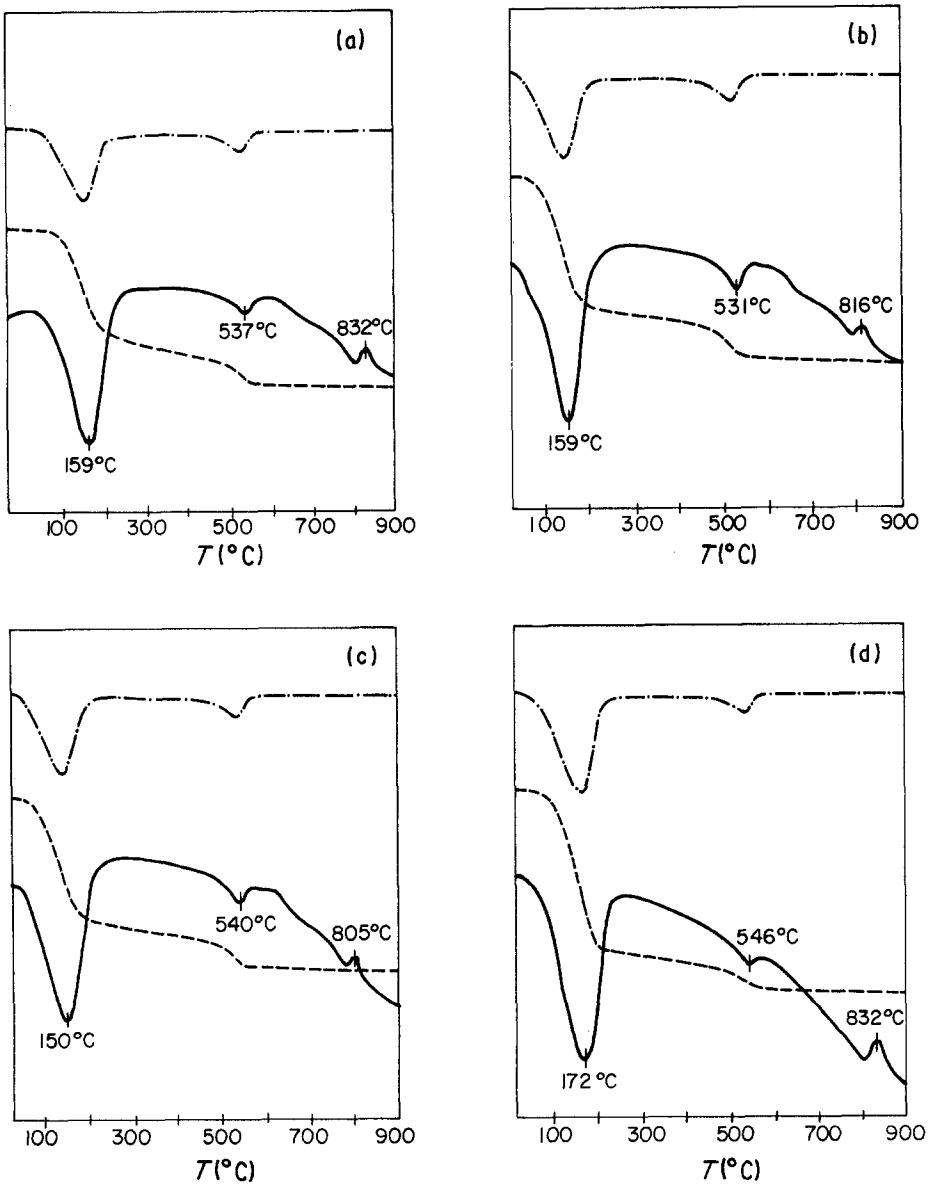


*Figure 3* DTA–TGA diagrams of the gels: (——) DTA, (– – –) thermogravimetry (TG), (–·–) derivative (TG). (a) 4.1, (b) 4.2, (e) 4.3, (d) 4.4.

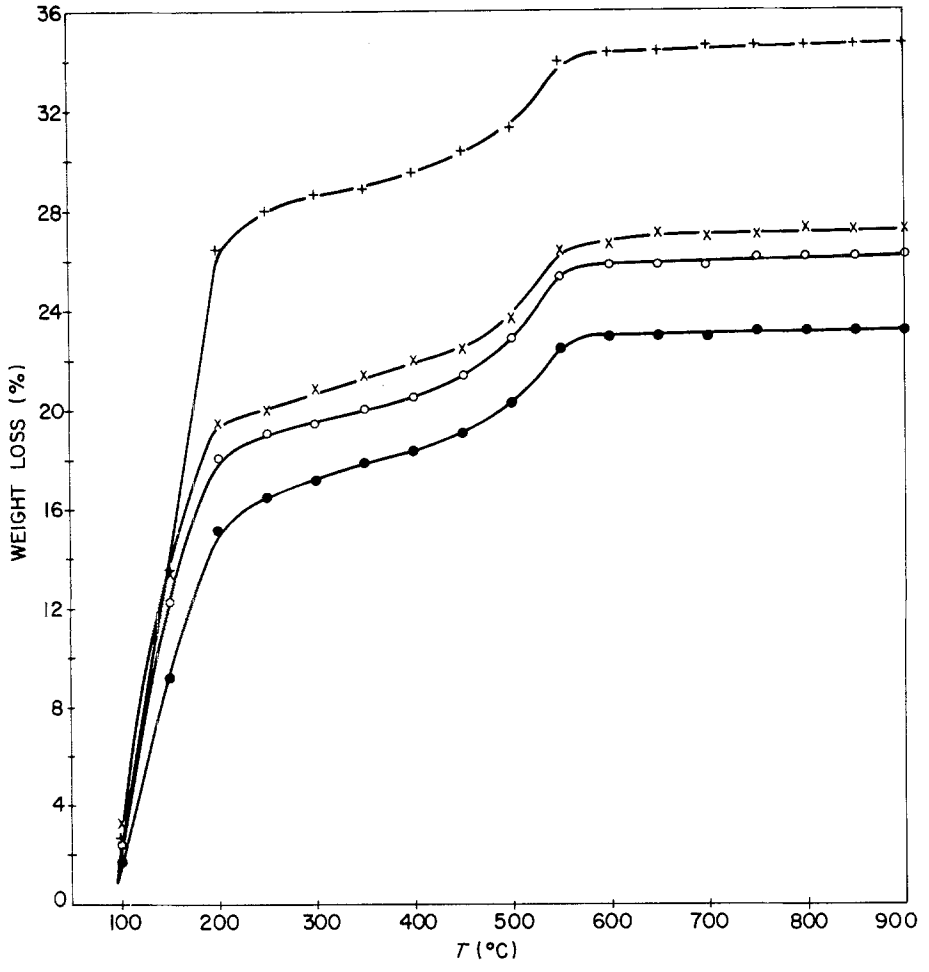


*Figure 4* Weight losses of the gels as a function of temperature: (●) 4.1, (○) 4.2, (×) 4.3, (+) 4.4.

confirmed by the data obtained from specific surface area and density measurements (Section 3.2.). Following loss of the chemically bonded water, a ponderal stabilization can be observed in the TG curves. In the temperature range between 805 and 832° C an exothermic peak appears which is not accompanied by any weight loss in the TG curves. These peaks in the DTA diagrams are due to a crystallization process, as evidenced by the X-ray diffraction data (Table III). The presence of water (residual ≡Si–OH and =B–OH groups) favours, as it were, reordering of the network towards incipient crystalline phases between 500 and 600° C, as well as ensuring α-cristobalite and tridymite crystallization at higher temperatures. Fig. 4 shows the weight losses computed from the TG curves as a function of temperature.

## 3.2. Specific surface area and density measurements

Fig. 5 represents the variation of density in the gels as a function of heat-treatment temperature. Up to 400° C, the sample densities vary only slightly, due to the fact that the basic process taking place is the release of adsorbed water hydrogen-bonded from ≡Si–OH and =B–OH groups and the loss of organic groups. Above 450° C the density increases much more rapidly, reaching its maximum at 600° C.

TABLE III X-ray diffraction data* for samples treated at different temperatures

| T (°C) | 4.1† | 4.2 | 4.3 | 4.4 |
|---|---|---|---|---|
| 120 to 600 | – | – | – | – |
| 750 to 850 | ×× + | ×××++ | ××+++ | ×××+++ |

*(–) Amorphous, (×) low α-cristobalite content, (××) moderate α-cristobalite content, (×××) high cristobalite content, (+) low tridymite content, (++) moderate tridymite content, (+++) high tridymite content.
†Composition No. (Table I).

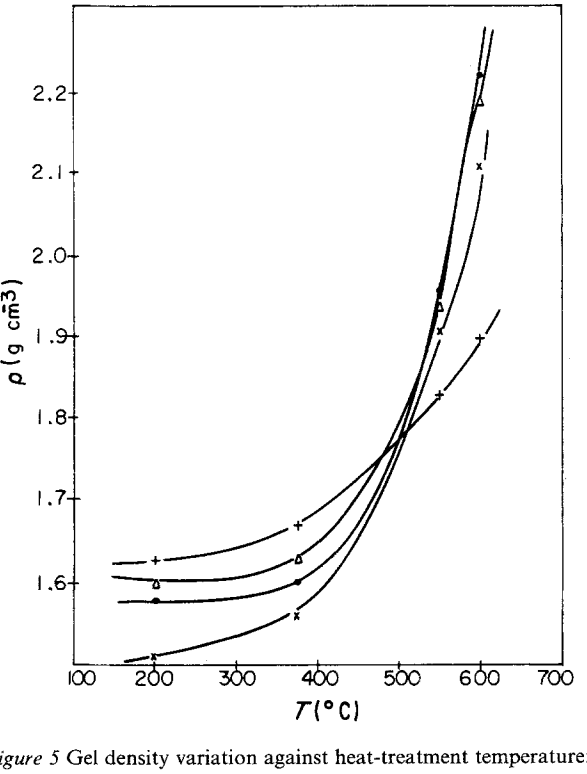


*Figure 5* Gel density variation against heat-treatment temperature: (●) 4.1, (×) 4.2, (+) 4.3, (△) 4.4.

TABLE IV Specific surface areas of gels treated at 200° C

| Composition No. | 4.1 | 4.2 | 4.3 | 4.4 |
|---|---|---|---|---|
| Specific surface area ($m^2 g^{-1}$) | 214.2 | 246.4 | 290.2 | 298.6 |

This latter temperature actually marks maximum gel densification prior to the onset of the crystalline restructuring process of the silica, which, at higher temperatures, enhances the appearance of α-cristobalite and tridymite.

The specific surface area data of the gels treated at 200° C (Table IV) fluctuate between 200 and 300 $m^2 g^{-1}$. An increase in specific surface area is observed, proportionate to a higher $SiO_2$ content and/or reduction of $B_2O_3$ levels. On increasing the silica content a $B_2O_3$ molecule is replaced by an $SiO_2$ molecule, which implies that one silicon atom replaces two boron atoms. Hence the number of ≡Si–OH groups increases and the network opens up, thus giving rise to larger specific surface area values. Moreover, specific surface area measurements were carried out on samples treated at low temperatures (200° C), where most of the $OH^-$ had not yet been eliminated. The $OH^-$ groups contribute significantly to the structural features of the gel, especially at 200° C, being responsible for many discontinuities in the more or less polymeric network making up the gel particles.

With regard to specific surface area variation as a function of temperature, measurements referring to the gel of Composition 4.4 in the range of 200 to 600° C (Fig. 6) were performed. Specific surface area data do not show any significant changes up to approximately 400° C, where there is an abrupt drop to 20 $m^2 g^{-1}$. In Fig. 6 both density variation and specific surface area for the gel 4.4 have been plotted against temperature The material is shown to begin to sinter at about 500° C, this process being complete around 600° C (maximum density and minimum specific surface area). This sintering temperature is relatively low, considering that for pure silica gels it occurs around 1000° C. The explanation for this difference can, however, be sought in the preparation method. In fact, an acid-catalysed hydrolysis, as was employed in this research, results in the formation of very small particles which sinter at relatively low temperatures.

### 3.3. IR and NIR spectra

Fig. 7 shows the IR spectra (400 to 2000 $cm^{-1}$) of the 4.1 gel heat-treated at different temperatures, as well as that referring to the glass of the same composition. The respective spectra of the other gels are similar, their evolution with temperature being practically identical to that of gel 4.1. This fact is self-explanatory, considering the compositional proximity of the four samples.

The absorption band presenting in all spectra near 460 $cm^{-1}$ is assigned [30–35] to the deformation vibration of the O–Si–O bonds. In the 4.1 glass spectrum a band can be observed around 690 $cm^{-1}$ attributable to the Si–O–B deformation vibration [34–37]. The bending vibration of the O–Si–O link [30] is situated around 800 $cm^{-1}$ and was observed for both the glass and the gels at all test temperatures. This band has also been assigned to the vibrations of tetrahedron rings ($SiO_4$) [33–35] and to asymmetric Si–O–stretching [37].

The Si–O–B vibration band which appears at 915 $cm^{-1}$ is not observed in the gel treated at 200° C, but begins to become visible in the samples treated at 550 and 600° C, becoming more intense with increasing temperature, which could be indicative of the fact that the densifying gel gives rise to mixed Si–O–B links. In the respective conventional glass spectrum this band is much more marked. The band presenting near 950 $cm^{-1}$ in the spectrum of the gel 4.1 treated at 200° C has been attributed [30] to residual OR groups. This band practically disappears at higher temperatures. The band observed for all spectra at 1090 $cm^{-1}$ is assigned

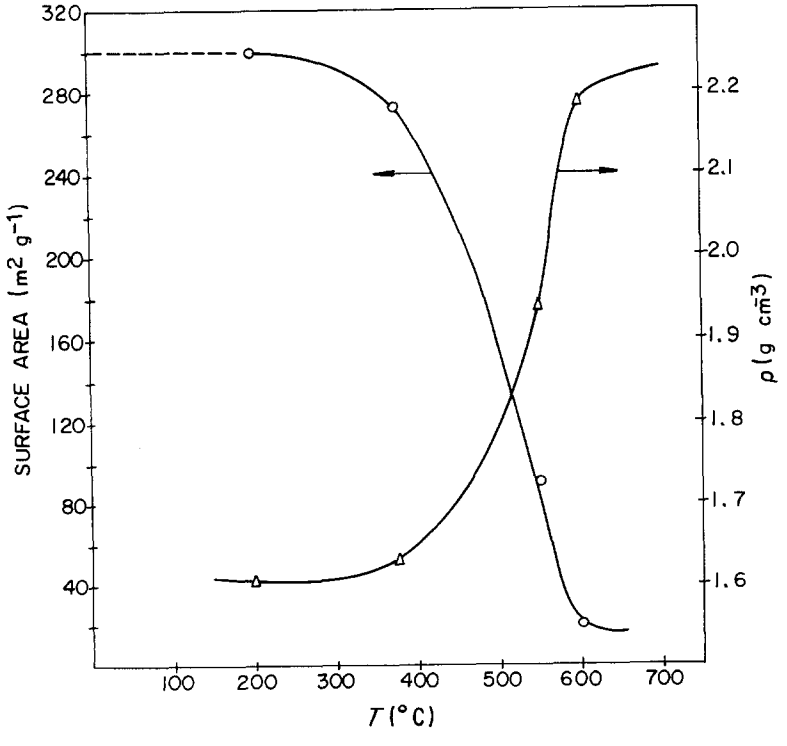


*Figure 6* Density and specific surface area evolution of gel 4.4 against heat-treatment temperature.

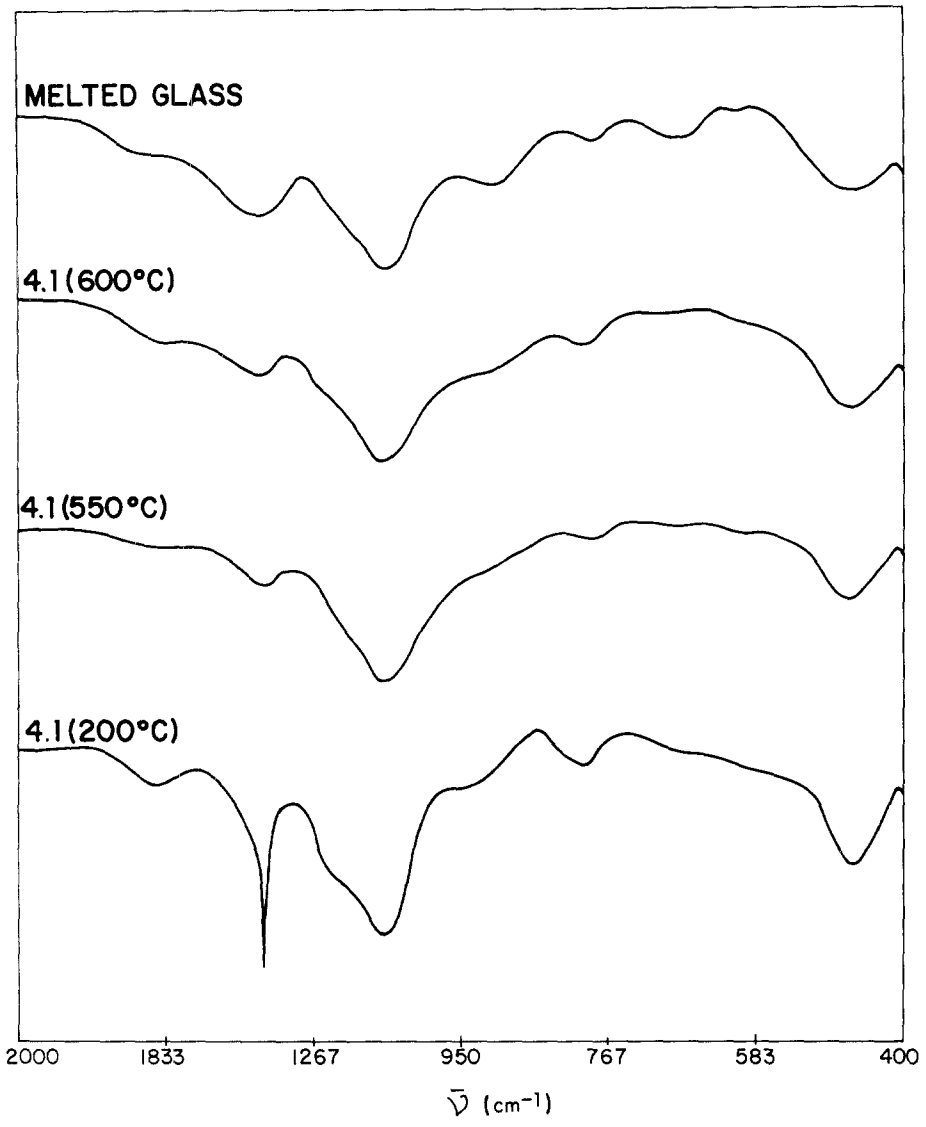


*Figure 7* IR spectra of gel 4.1 (200, 550 and 600° C) and glass of the same composition.

[18, 25, 26, 30, 33–37] to the asymmetric Si–O stretching vibration.

The gel 4.1 (200° C) presents a shoulder at approximately 1160 cm$^{-1}$ attributable [30] to residual OR groups and an acute band at 1385 cm$^{-1}$ due to the C–H deformation vibration of the methyl group. Both bands disappear with increasing temperature, because all organic groups are eliminated before reaching 500° C, as stated in Section 3.1.

Finally, at 1400 cm$^{-1}$, there appears a band in the

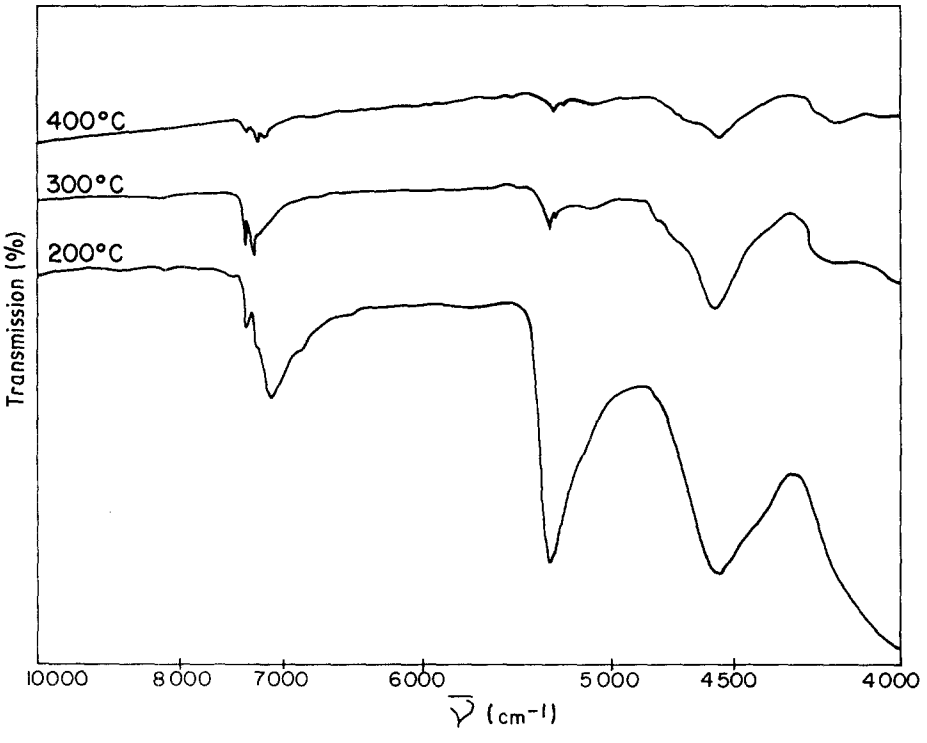


*Figure 8* NIR spectra of gel 4.1 (200, 300 and 400° C).

spectra of the gel treated at 550 and 600° C, as well as in the spectrum obtained for the glass 4.1, attributable [30, 36, 37] to B–O stretching vibration.

The most relevant observation in Fig. 7 refers to the spectral similarity between the gel 4.1 treated at 600° C (maximum densification) and the conventional glass of the same composition. This fact allows us to conclude that the bonds of the sintered gel are similar to those of the glass prepared by conventional melting.

NIR spectroscopy has proved to be a useful tool in the study of the thermal evolution of water and silanol groups, both in conventional glasses [39–43] and gels [44–46].

Fig. 8 shows the NIR spectra (4000 to 10 000 $cm^{-1}$) of the gel 4.1 treated at 200, 300 and 400° C. The spectra of the remaining samples present the same bands as those observed for the gel 4.1, for the same reason as that given for the IR spectra.

Three groups of bands can be differentiated, located around 4500, 5300 and 7300 $cm^{-1}$. The broad band at 4545 $cm^{-1}$ is assigned to the stretching–bending combination vibration of the O–H bonds of the free silanol groups, as observed in fused silica glass [39] and in silicate glasses [40–43]. This band was also assigned [44] to the same vibration mode of silanol groups hydrogen-bonded to water molecules (Fig. 9a). This band is observed to diminish markedly on temperature increase, due to almost total molecular water release around 400° C and the onset of network closure due to the condensation of silanol groups.

The bands at 7194 and 5295 $cm^{-1}$ correspond, respectively, to the first overtone [44, 45] and to the stretching–bending combination vibration of the water molecules hydrogen-bonded to neighbouring silanol groups [41–44] (Fig. 9a). The evolution of both bands is similar and indicates the elimination of the physically adsorbed water, which is virtually complete at 400° C.

The band corresponding to the first overtone of O–H stretching vibration of the free isolated silanol groups appears at 7305 $cm^{-1}$ [39, 41–44] (Fig. 9c), and that pertaining to the free neighbouring silanol at 7342 $cm^{-1}$ [44] (Fig. 9). Both silanol groups, neighbouring and isolated, follow the same thermal evolution. At 300° C no significant diminishment is observed in the bands, due to the fact that, in spite of adsorbed water release, there still remain a considerable number of silanols in the situation represented in Figs. 9b and c. Later on, at 400° C, the bands at 7305 and 7342 $cm^{-1}$ diminish, due to the onset of the sintering process, which causes network closure.

It proved impossible to record NIR spectra for the gel slab heat-treated above 400° C, due to the failure to prepare crack-free samples at these higher temperatures.

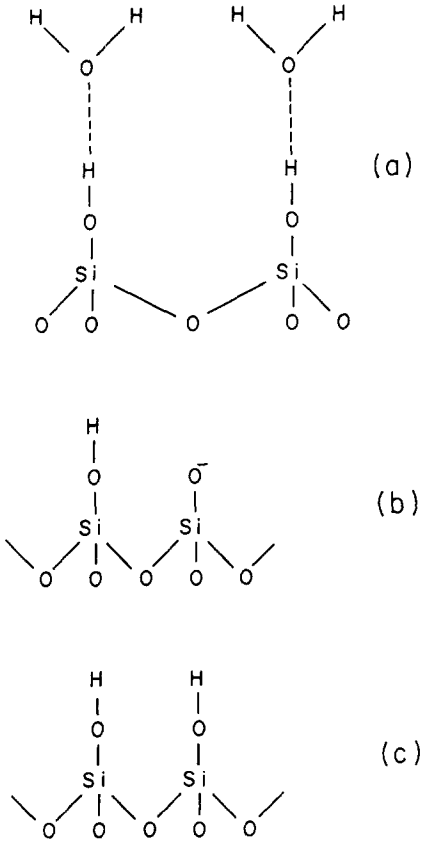


*Figure 9* Schematic representation of the molecular structures present in a pure silica gel according to Wood *et al.* [44].

## 3.4. Gel microstructure

The texture of gels treated at 200° C was studied by SEM. Fig. 10 shows the aspect of sample 4.1. at 200° C. In the micrographs of the other three gels a slightly granulated, but fairly homogeneous structure can likewise be observed.

The microstructure of the gel 4.1 densified at 600° C (original gel before phase separation by inductive heat-treatment) was observed by means of TEM. Fig. 11a shows a homogeneous distribution of very small droplets. In certain isolated areas of the sample, however, there appear crystalline formations (Fig. 11b) attributable to incipient devitrification of the silica. Devitrification becomes massive around 850° C, as confirmed by DTA data (Fig. 3) and X-ray diffraction data (Table III).

The transmission micrographs of the glass 4.1 obtained by conventional melting (original tempered glass) show certain similarities to the micrographs in Fig. 11, with the exception that there do not appear to

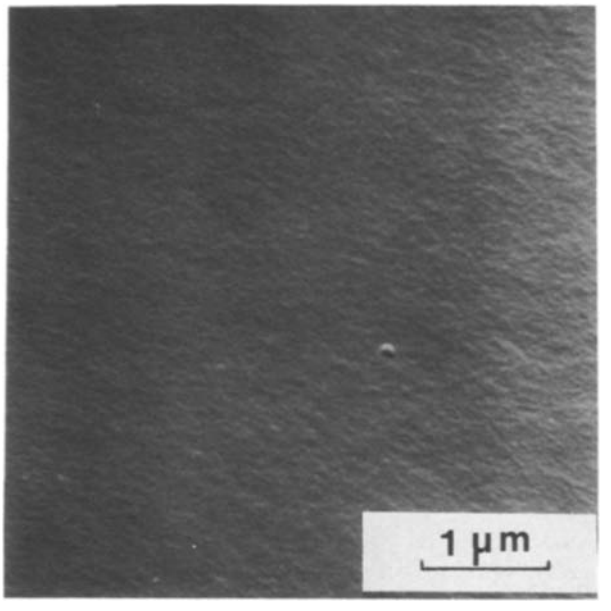


*Figure 10* SEM micrograph of 4.1 gel treated at 200° C.

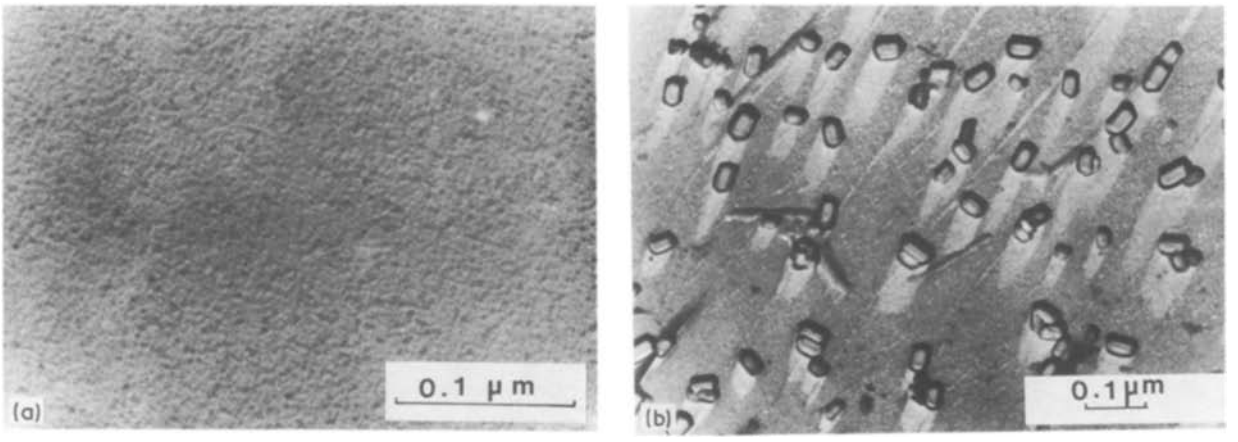


*Figure 11* TEM micrographs of gel 4.1 densified at 600° C. (a) Homogeneous aspect of the sample; (b) aspect of an isolated zone with crystalline formations.

be any crystalline formations in the glass, which presents, however, a more accurately defined texture than the gel. In Fig. 13 a homogeneous microstructure can be observed.

With the aim of investigating the possible existence of the phenomenon of phase separation in the glass 4.1 at relatively low temperatures, two heat-treatments at 500° C were performed. Fig. 13 shows the microstructure of the conventional glass, heat-treated at 500° C for 2 h (Fig. 13a) and 6.5 h (Fig. 13b), which proves to be practically identical to that of the original tempered glass (Fig. 12). This provides evidence of the fact that at 500° C phase separation has not yet occurred.

TEM observation of the gel 4.1 and the glass of the same composition, which were both simultaneously heat-treated for 12 h at 600° C (Fig. 14), demonstrate the existence of an incipient phase separation in the gel and even more markedly in the glass. It must be taken into account that the gel 4.1, whose microstructure is shown in Fig. 14a, has undergone a much longer heat-treatment than the glass, considering that, in addition to the 12 h of joint-treatment, the gel had been pre-heated for another 12 h at that very temperature during the densification process (Section 2.2). Hence and with regard to the experimental conditions, the truly comparable samples would be the gel in Fig. 11 and the glass in Fig. 14.

After simultaneous 4-hour heat-treatment of the gel 4.1 and glass at 700° C a straightforward phase separation was observed in the conventional glass, as evidenced by TEM micrographs (Fig. 15). By contrast, the microstructure of the gel 4.1 after this latter treatment (Fig. 16) shows droplets which furthermore promote a phase separation, though less pronounced or delayed with regard to the phenomenon in the glass. Fig. 16 shows the thermal evolution of a zone which, at lower temperatures, had presented crystallization nuclei.

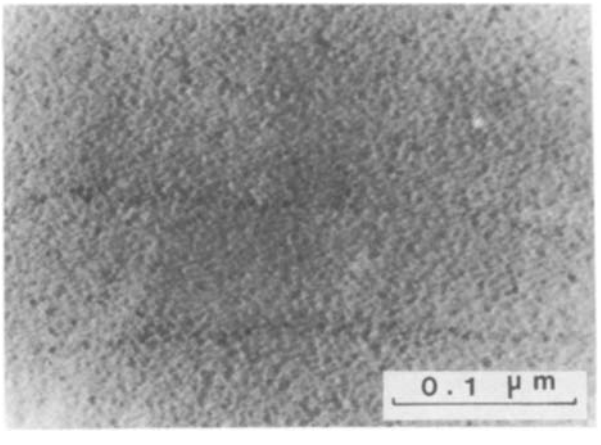


*Figure 12* TEM micrograph of conventional tempered glass 4.1.

The results obtained are consistent with the findings of other authors [31] although perhaps not totally comparable, as these latter are related to glasses prepared by gel melting processes. Nevertheless, apart from the fact that the homogeneity of glasses derived from gels through melting is different from that of conventional glasses [31, 32], this research demonstrates significantly that gels densified below the glass transition temperature present a more uniform microstructure and particle distribution than the respective conventional glasses.

Weinberg and Neilson [32] have explained the phenomenon of separate phases in glasses derived from gels of the system $Na_2O$–$SiO_2$ through melting as a function of the greater water content of these materials with regard to conventional glasses. As a matter of fact, the presence of water in the form of $OH^-$ groups tends to break the vitreous network, yielding a lower degree of polymerization of the $SiO_2$ units, which causes the composition to move towards the spinodal region. As a result, a stronger phase separation takes place than in the case of glasses prepared by conventional melting. By the same token, Mukherjee *et al.* [31] attribute the increase in nucleation and crystallization rates to the presence of residual $OH^-$ groups in the gel, which were subsequently incorporated into the resulting glass structure.

In this research the gels were not melted. They were densified and then heat-treated at different temperatures to enhance phase separation. Hence the thermal histories of the gels and the glass are not identical. The present work allows us, however, to gain knowledge about gel behaviour (densified but without reaching the melting point) parallel to that of conventional glass. The results indicate that, on heat-treatment, despite the high water content, the phase separation phenomenon, although it is not inhibited, is clearly

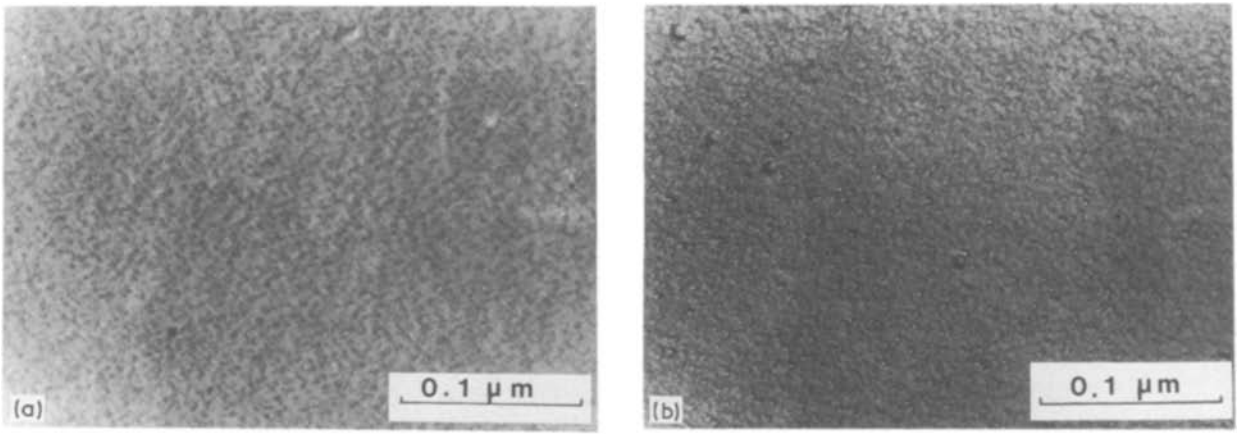


*Figure 13* TEM micrographs of 4.1 glass heat-treated at 500° C for (a) 2 h and (b) 6.5 h.

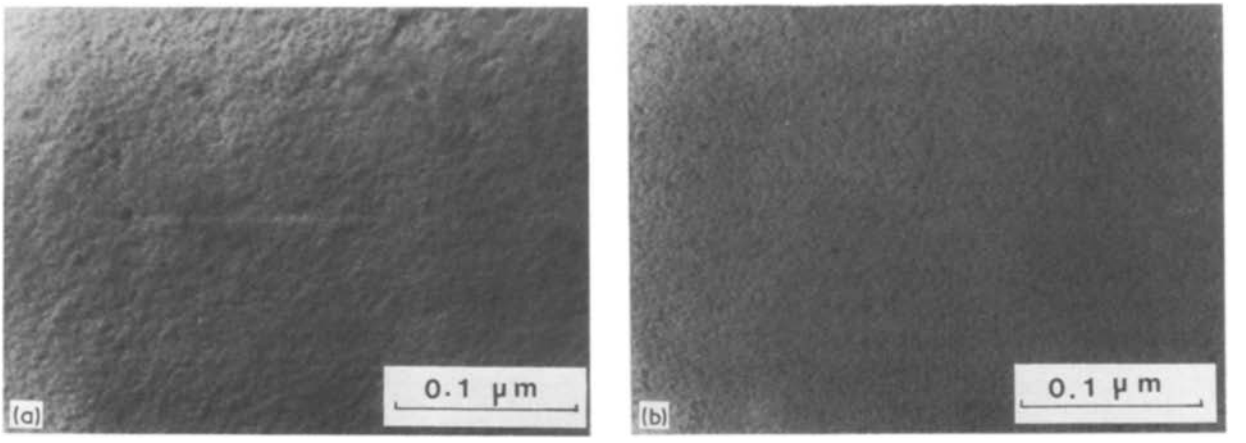


*Figure 14* TEM micrographs taken after 12 h heat-treatment at 600° C for (a) gel 4.1 and (b) conventional glass of the same composition.

delayed or attenuated. On the other hand, for the gels the appearance of crystallization nuclei must be taken into account, which are doubtlessly caused by the presence of water. The fact that the gel 4.1 after heat-treatment does not present a more marked phase separation than the glass of the same composition could be attributable to the thermal history of that gel, free of any melting incident.

## 4. Conclusions

As evidenced in the DTA–TGA diagrams, the samples follow the typical thermal evolution of materials prepared by the sol–gel process. The first event to occur is the loss of physically adsorbed water, followed by O–H elimination from the ≡Si–OH and =B–OH groups and ending up in silica crystallization due to the presence of relatively large amounts of water in the form of residual ≡Si–OH and =B–OH groups.

Although NIR spectra at 400° C show incipient dehydroxylation due to condensation of the ≡Si–OH and =B–OH groups and the onset of densification, a sufficiently densified glass structure is not achieved until reaching temperatures above 550 to 600° C. Even at these temperatures there continue to exist residual ≡Si–OH and =B–OH groups which favour further crystallization of α-cristobalite and tridymite.

The structural evolution of the gels is slow up to 400° C, as only adsorbed water and organic groups are lost during this range of temperature. At higher temperatures than 400° C significant density and specific

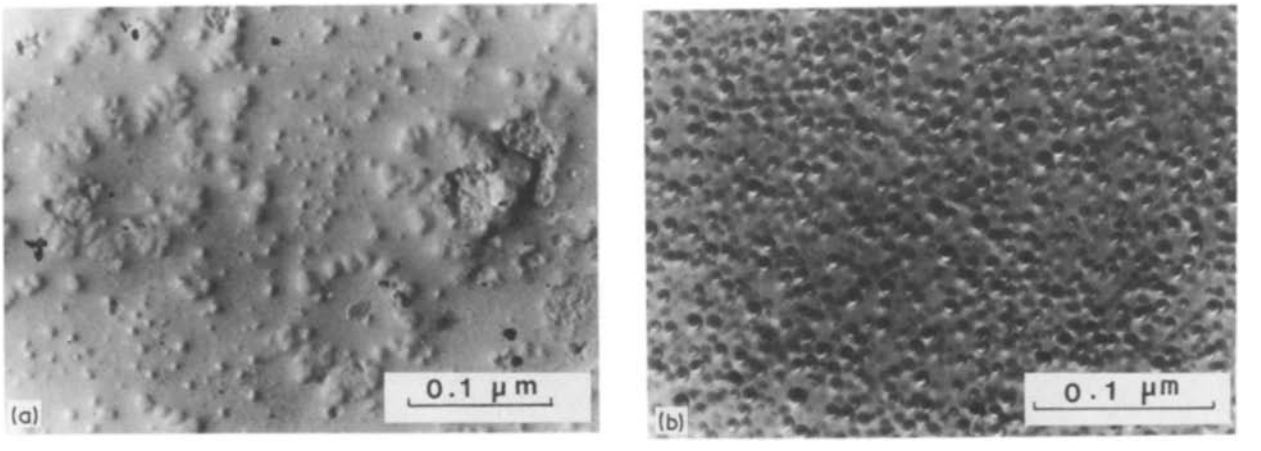


*Figure 15* TEM micrographs of glass 4.1 heat-treated at 700° C for 4 h.

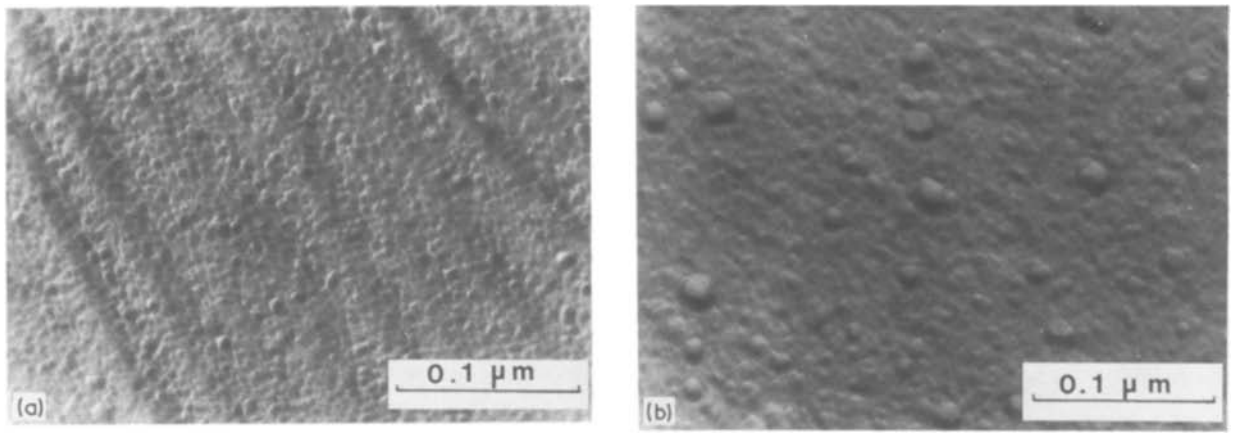


*Figure 16* TEM micrographs of gel 4.1 heat-treated at 700° C for 4 h. (a) Granular aspect of the representative sample area; (b) aspect of the evolution of an isolated area with crystalline formations.

surface area of variations indicate the presence of a process similar to sintering. The structure of the samples at 600° C is similar to that of the respective glasses prepared by conventional melting, as confirmed by the IR spectroscopy data.

Above 600° C the onset of the phase separation phenomenon was observed in gels, analogous to the phenomenon in one of the glasses of identical composition prepared by conventional melting, although for gels considerably longer heat-treatment times are required. In the gels this phenomenon is less than in glasses. In this respect it is important to bear in mind that the presence of water in the gels is mainly responsible for their readiness to crystallize or devitrify above 600 to 700° C.

## References


1. M. NOGAMI and Y. MORIYA, *J. Non-Cryst. Solids* **37** (1980) 191.
2. C. J. BRINKER, K. D. KEEFER, D. W. SHAEFER and C. S. ASHLEY, *ibid.* **48** (1982) 47.
3. L. C. KLEIN and G. J. GARVEY, *ibid.* **48** (1982) 97.
4. P. YU, H. LIU and G. WANG, *ibid.* **52** (1982) 511.
5. C. J. BRINKER, K. D. KEEFER, D. W. SHAEFER, R. A. ASSINK, B. D. KAY and C. S. ASHLEY, *ibid.* **63** (1984) 45.
6. T. KAWAGUCHI, J. IURA, N. TANEDA, H. HISHIKURA and Y. KOKUBU, *ibid.* **82** (1986) 50.
7. D. L. WOOD and E. M. RABINOVICH, *ibid.* **82** (1986) 171.
8. J. G. van LIEROP, A. HUIZING, W. C. P. M. MEERMAN and C. A. M. MULDER, *ibid.* **82** (1986) 265.
9. S. WALLACE and L. L. HENCH, *Mater. Res. Soc. Symp. Proc.* **32** (1984) 47.
10. T. WOIGNIER and J. PHALIPPOU, *Riv. della Staz. Sper. Vetro* **5** (1984) 47.
11. M. YAMANE, S. INOUE and A. YASUMORI, *J. Non-Cryst. Solids* **63** (1984) 13.
12. J. PHALIPPOU, T. WOIGNIER and J. ZARZYCKI, in "Ultrastructure Processing of Ceramics, Glasses and Composites", edited by L. L. Hench and D. R. Ulrich (Wiley, New York, 1984) p. 70.
13. K. SUSA, I. MATSUYAMA, S. SATOH and T. SUGANUMA, *J. Non-Cryst. Solids* **79** (1986) 165.
14. C. J. BRINKER and S. P. MUKHERJEE, *J. Mater. Sci.* **16** (1981) 1980.
15. J. PHALIPPOU, M. PRASSAS and J. ZARZYCKI, *J. Non-Cryst. Solids* **48** (1982) 17.
16. T. A. GALLO, C. J. BRINKER, L. C. KLEIN and G. W. SCHERER, *Mater. Res. Soc. Symp. Proc.* **32** (1984) 85.
17. F. PANCRAZI, J. PHALIPPOU, F. SORRENTINO and J. ZARZYCKI, *J. Non-Cryst. Solids* **63** (1984) 81.
18. N. THOGE, G. S. MOORE and J. D. MACKENZIE, *ibid.* **63** (1984) 95.
19. T. WOIGNIER, J. PHALIPPOU and J. ZARZYCKI, *ibid.* **63** (1984) 117.
20. S. P. MUKHERJEE and W. H. LOWDERMILK, *Appl. Optics* **21** (1982) 293.
21. S. SAKKA, K. KAMIYA and K. MAKITA, *J. Mater. Sci. Lett.* **2** (1983) 395.
22. E. M. RABINOVICH, J. B. MACCHESNEY, D. W. JOHNSON Jr, J. R. SIMPSON, B. W. MEAGHER, F. W. DIMARCELLO, D. L. WOOD and E. A. SIGETY, *J. Non-Cryst. Solids* **63** (1984) 155.
23. P. M. GLASER and C. G. PANTANO, *ibid.* **63** (1984) 209.
24. K. KAMIYA and T. YOKO, *ibid.* **21** (1986) 842.
25. S. P. MUKHERJEE, *ibid.* **42** (1980) 477.
26. *Idem*, in "Materials Processing in the Reduced Gravity Environment of Space", edited by G. E. Rindone (Elsevier, Amsterdam, 1982) p. 91.
27. *Idem, J. Non-Cryst. Solids* **63** (1984) 35.
28. S. P. MUKHERJEE and R. K. MOHR, *ibid.* **66** (1984) 523.
29. G. ORCEL and L. L. HENCH, *Mater. Res. Soc. Symp. Proc.* **32** (1984) 79.
30. C. J. BRINKER and D. M. HAALAND, *J. Amer. Ceram. Soc.* **66** (1983) 758.
31. S. P. MUKHERJEE, J. ZARZYCKI and J. P. TRAVERSE, *J. Mater. Sci.* **11** (1976) 341.
32. M. C. WEINBERG and G. F. NEILSON, *ibid.* **13** (1978) 1206.
33. M. DECOTTIGNIES, J. PHALIPPOU and J. ZARZYCKI, *ibid.* **13** (1978) 2605.
34. R. JABRA, J. PHALIPPOU and J. ZARZYCKI, *Rev. Chim. Min.* **16** (1979) 245.
35. M. PRASSAS and L. L. HENCH, in "Ultrastructure Processing of Ceramics, Glasses and Composites", edited by L. L. Hench and D. R. Ulrich (Wiley, New York, 1984) p. 100.
36. M. NOGAMI and Y. MORIYA, *J. Non-Cryst. Solids* **48** (1982) 359.
37. D. M. HAALAND and C. J. BRINKER, *Mater. Res. Soc. Symp. Proc.* **32** (1984) 267.
38. A. BERTOLUZZA, C. FAGNANO, M. A. MORELLI, V. GOTTARDI and M. GUGLIELMI, *J. Non-Cryst. Solids* **48** (1982) 117.
39. D. L. DODD and D. B. FRASER, *J. Appl. Phys.* **37** (1966) 3911.
40. C. K. WU, *J. Amer. Ceram. Soc.* **63** (1980) 453.
41. R. F. BARTHOLOMEW, B. L. BUTLER, H. L. HOOVER and C. K. WU, *ibid.* **63** (1980) 481.
42. R. F. BARTHOLOMEW, *J. Non-Cryst. Solids* **56** (1983) 331.
43. J. ACOCELLA, M. TOMOZAWA and E. B. WATSON, *ibid.* **65** (1984) 355.

44. D. L. WOOD, E. M. RABINOVICH, D. W. JOHNSON Jr, J. B. MACCHESNEY and E. M. VOGEL, *J. Amer. Ceram. Soc.* **66** (1983) 693.
45. F. ORGAZ and H. RAWSON, *J. Non-Cryst. Solids* **82** (1986) 57.
46. M. A. VILLEGAS and J. M. FERNANDEZ NAVARRO, *Bol. Soc. Esp. Ceram. Vidr.* **26** (1987) 235.

*Received 22 June*
*and accepted 22 September 1987*